

## Recoil Properties of Radionuclides Formed in Photonuclear Reactions on $^{197}\text{Au}$ at Intermediate Energies

H. Haba,<sup>\*,a</sup> M. Igarashi,<sup>b</sup> K. Washiyama,<sup>a</sup> H. Matsumura,<sup>a</sup> M. Yamashita,<sup>a</sup>  
K. Sakamoto,<sup>†,a,b</sup> Y. Oura,<sup>c</sup> S. Shibata,<sup>d</sup> M. Furukawa,<sup>e</sup> and I. Fujiwara<sup>f</sup>

<sup>a</sup>Division of Physical Sciences, Graduate School of Natural Science and Technology, Kanazawa University, Kanazawa-shi, Ishikawa 920-1192, Japan

<sup>b</sup>Department of Chemistry, Faculty of Science, Kanazawa University, Kanazawa-shi, Ishikawa 920-1192, Japan

<sup>c</sup>Department of Chemistry, Graduate School of Science, Tokyo Metropolitan University, Hachioji-shi, Tokyo 192-0397, Japan

<sup>d</sup>Research Reactor Institute, Kyoto University, Sennan-gun, Osaka 590-0494, Japan

<sup>e</sup>Faculty of Environmental and Information Sciences, Yokkaichi University, Yokkaichi-shi, Mie 512-8512, Japan

<sup>f</sup>Department of Economics, Faculty of Economics, Otomon-Gakuin University, Ibaraki-shi, Osaka 567-8502, Japan

Received: April 4, 2000; In Final Form: September 18, 2000

The recoil properties of 37 radionuclides with the mass number  $A = 24\text{--}131$  produced in the photonuclear reaction on  $^{197}\text{Au}$  by bremsstrahlung of end-point energies ( $E_0$ ) from 300 to 1100 MeV have been investigated using the thick-target thick-catcher method with an aid of intensive chemical separations. The measured mean ranges,  $FW$  and  $BW$ , in the forward and backward directions, respectively, with respect to the beam axis show  $E_0$ -independence above 600 MeV, reflecting the resonance character in photonuclear reactions at intermediate energies. The forward-to-backward yield ratios ( $F/B$ ) are independent of the mass difference ( $\Delta A$ ) between a product ( $A$ ) and the target ( $A_t = 197$ ) above  $\Delta A = 66$ , and the weighted mean value of  $F/B = 1.1 \pm 0.1$  is clearly distinguished from that of photospallation products with  $\Delta A \leq 45$ . The  $F/B$  ratios of proton-induced reactions at incident proton energies ( $E_p$ ) of  $E_p \leq 3$  GeV are higher than those of photon-reactions and decrease with an increase of  $E_p$ , but become the same values as the photon-reactions at higher  $E_p$ . The mean kinetic energies  $T$  of the residual nuclei were deduced based on the two-step vector velocity model. The  $T$  values are independent of  $E_0$  above 600 MeV and increase with an increase of  $\Delta A$ , reflecting the changes in the reaction mechanism from spallation to fission. The  $T$  values of photon-reactions at  $\Delta A > 45$  are quite different from those of the proton-reactions, in which the  $T$  values decrease with an increase of  $E_p$  up to about 3 GeV and become  $E_p$ -independent at higher  $E_p$ , though the  $T$  values of photon-reactions at  $\Delta A \leq 45$  agree well with those of the proton-reactions, irrespectively of  $E_p$ . Recoils of  $^{24}\text{Na}$  produced from  $^{27}\text{Al}$ ,  $^{nat}\text{V}$ ,  $^{nat}\text{Cu}$ ,  $^{nat}\text{Ag}$ , and  $^{197}\text{Au}$  are of special interest from a viewpoint of a change in the production mechanism with respect to  $A_t$ .

### 1. Introduction

Photons are the force carriers of the electromagnetic interaction. The electromagnetic force can act on the scale of the whole nucleus but also on the smaller scale of nucleons, and so this interaction is very useful for probing both global and local properties of the atomic nucleus. At intermediate energies, photons interact with the nucleus through three main processes; giant dipole resonance, quasi-deuteron mechanism, and (3,3) resonance, which are characteristic for the wavelength of incident photons. These initial interactions are quite different from that of hadron-induced reactions initiated by the strong nucleon-nucleon interaction. It is of interest to investigate whether there exist similarities or not in the final steps in these two types of nuclear reactions.

We have been measuring the yields of bremsstrahlung-induced reactions such as photospallation,<sup>1–4</sup> photofragmentation,<sup>5,6</sup> photofission,<sup>7</sup> and photopion reaction<sup>8–11</sup> from  $^7\text{Li}$  to  $^{209}\text{Bi}$  targets in order to establish the systematics of photonuclear reactions and to investigate the reaction mechanism and nuclear structure. Fruitful information about these aspects has been obtained from yield measurements so far. Further experiments using a nuclear recoil technique are expected to give us

information such as angular distributions and kinetic energies of product nuclei, and to deepen our understanding on the reaction mechanism.

Recently, recoil properties of radionuclides formed in the photospallation reactions on  $^{27}\text{Al}$ ,  $^{nat}\text{V}$ ,  $^{nat}\text{Cu}$ ,  $^{93}\text{Nb}$ ,  $^{nat}\text{Ag}$ ,  $^{nat}\text{Ta}$ , and  $^{197}\text{Au}$  at bremsstrahlung of end-point energies ( $E_0$ ) from 600 to 1100 MeV were successfully investigated using the thick-target thick-catcher method.<sup>12–14</sup> Reflecting the resonance character in a photonuclear reaction, the mean ranges  $FW$  and  $BW$  in the forward and backward directions with respect to beam axis are  $E_0$ -independent at the studied energies and they increase with an increase of the mass difference ( $\Delta A$ ) between a product ( $A$ ) and the target ( $A_t$ ), showing two components of the  $(\gamma, xnyp)$  ( $x, y \geq 1$ ) and the  $(\gamma, xn)$  ( $x \geq 1$ ) reactions. The forward-to-backward ratios ( $F/B$ ) are independent of  $\Delta A$  as well as the targets ( $F/B = 2\text{--}3$ ). The kinematic properties of the product nuclei were analyzed by the two-step vector velocity model.<sup>15</sup> The forward velocity  $v$  after the first step of photon-reaction is quite different from that of proton-reaction at incident proton energies of  $E_p \leq 3$  GeV, though the difference disappears at higher energies. On the other hand, the mean kinetic energy  $T$  of the residual nucleus in the second step is almost equal to that of proton-reaction irrespectively of  $E_p$ . A comparison with  $T$  values calculated by the photon-induced intranuclear cascade analysis code (PICA) by Gabriel and Alsmiller<sup>16,17</sup> was also performed at  $E_0 = 400$  MeV. It was found that although the code well reproduces the experimental results of  $^{nat}\text{V}$  and  $^{nat}\text{Cu}$ , the same calculation for heavier

\*Present address: Japan Atomic Energy Research Institute, Tokai-mura, Naka-gun, Ibaraki 319-1195, Japan. E-mail: haba@popsvr.tokai.jaeri.go.jp.

†Corresponding author. E-mail: kohsakamoto@par.odn.ne.jp. FAX: +81-76-224-8253.

targets gives  $T$  values lower than the experimental results, indicating some nuclear-structure effect, such as a medium effect notably at  $A_i \geq 100$ . An average kinetic energy carried off by the emitted particles  $\varepsilon_s = T/(\Delta A/A_i)$  of both photon- and proton-reactions seem to increase with an increase of  $A_i$  up to around  $A_i = 100$ , and become almost constant at larger  $A_i$ , implying also some change in the nuclear structure effect in this heavy target region, as also found in our recent yield measurements of photospallation<sup>3</sup> and photopion reactions.<sup>11</sup> The  $\varepsilon_s$  values of photon-reaction appear to be slightly lower than those of proton-reactions for <sup>nat</sup>Ag, <sup>nat</sup>Ta, and <sup>197</sup>Au, indicating the lower excitation energy left after the first step in photon-reactions than in proton-reactions.

It was found from our systematic yield measurements that the target nucleus of <sup>197</sup>Au undergoes spallation,<sup>2,3</sup> fission,<sup>7</sup> and fragmentation,<sup>6</sup> which are dominant for the products with  $\Delta A < \sim 60$ ,  $\Delta A \sim 60\text{--}160$ , and  $\Delta A \sim 160$ , respectively. In the present work, the recoil properties of 37 radionuclides with  $\Delta A = 66\text{--}173$  have been obtained at a wide energy range of  $E_0 = 300\text{--}1100$  MeV using the thick-target thick-catcher method with an aid of chemical separations in order to investigate photofission and photofragmentation processes dynamically. The present results together with those of the photospallation<sup>14</sup> are discussed as a whole by referring to the literature values on the proton-induced reaction, and to the calculated ones by the PICA code.<sup>16,17</sup> Recently, the yields of light nuclei such as <sup>7,10</sup>Be, <sup>22,24</sup>Na and <sup>28</sup>Mg from 23 targets of <sup>nat</sup>B to <sup>197</sup>Au were measured,<sup>6</sup> and it was found that their  $A_i$ -dependence shows two components of photospallation and photofragmentation. In the present paper, recoils of <sup>24</sup>Na produced from <sup>27</sup>Al, <sup>nat</sup>V, <sup>nat</sup>Cu, <sup>nat</sup>Ag, and <sup>197</sup>Au are of special interest from a viewpoint of a change in the production mechanism with respect to  $A_i$ . The present recoil technique accompanied by the chemical separations was powerful to determine low fission yields of <sup>197</sup>Au and to investigate detailed fission properties such as charge and mass distributions. The absolute yields of the 58 products in the mass range of  $42 \leq A \leq 131$  were reported in the separate paper.<sup>7</sup>

## 2. Experimental

Irradiations by electron-free bremsstrahlung beams with  $E_0 = 300\text{--}1100$  MeV in steps of 100 MeV or less were carried out using the 1.3 GeV electron synchrotron of the High Energy Accelerator Research Organization (KEK) at Tanashi. A 50

$\mu\text{m}$  thick Pt foil was used as a radiator for bremsstrahlung production, and the beam was collimated to 20 mm in diameter at the irradiation position. The target consisted of a stack of 40–50 sets of a Au foil (99.99%) of 90 mg/cm<sup>2</sup> in thickness and  $2.5 \times 2.5$  cm<sup>2</sup> in size sandwiched by one pair of Mylar foil of 7.0 mg/cm<sup>2</sup> in thickness and  $2.5 \times 2.5$  cm<sup>2</sup> in size, which collected the recoil nuclei in the forward or backward directions with respect to the beam axis. The stack was vacuum-encapsulated in a polyethylene bag together with additional 40–50 Mylar foils (280–350 mg/cm<sup>2</sup>) on the downstream side of the beam, which served as an activation blank. Details of the irradiation were almost the same as described in the previous papers.<sup>1,8,9</sup> The photon intensities evaluated from the monitor reaction of <sup>27</sup>Al( $\gamma,2\text{pn}$ )<sup>24</sup>Na (Refs. 18, 19) were  $10^9\text{--}10^{10}$  equivalent quanta per second (eq.q./s). A typical irradiation period was 5 h.

After irradiation, about 10 selected Au foils and all of the forward and backward catcher foils from one target pile were collected separately and were assayed for radioactivities nondestructively with high-purity Ge detectors each coupled with a 4 k-channel pulse height analyzer. The other 30–40 Au foils were divided into three portions and subjected to the chemical separations of K, Fe, Ni, Zn, Ga, As, Rb, Sr, Y, Zr, Nb, Mo, Ag, and Ba. All of the chemical procedures applied in the present work were described in a separate paper.<sup>20</sup> Radioactivities in the chemically separated samples were assayed by  $\gamma$ -ray spectrometry. In order to extend the recoil data of products with low reaction yields, chemical separations of scandium and barium were employed for the Mylar catchers in a separate irradiation at  $E_0 = 1000$  MeV. The identifications of radionuclides were made on the basis of their  $\gamma$ -ray energies and half-lives. The  $\gamma$ -ray intensities were obtained with the automatic peak search program, "SPECAnal98" by Hamajima,<sup>21</sup> which is based on the original one by Komura.<sup>22</sup> The detector efficiency was determined with calibrated <sup>152</sup>Eu and <sup>182</sup>Ta sources with the same size as the samples. The decay properties of interest such as half-lives,  $\gamma$ -ray energies, and branching ratios<sup>23–25</sup> are summarized in Table 1, together with formation types; I: independent yield, C-: cumulative yield by  $\beta^-$  decay, and C+: cumulative yield by  $\beta^+$  decay and/or electron capture. This classification was based on charge distributions of the product nuclei,<sup>7</sup> irradiation periods, and times required for chemical separations. The contributions of the blank activities to the catcher foil were found to be negligible for all of the radionuclides of interest here.

TABLE 1: Relevant Nuclear Data

Nuclide	Half life	$E_\gamma(\text{keV})$	b.r.(%)	TYPE	Detec. <sup>*4</sup>	Nuclide	Half life	$E_\gamma(\text{keV})$	b.r.(%)	TYPE	Detec.	Nuclide	Half life	$E_\gamma(\text{keV})$	b.r.(%)	TYPE	Detec.
Ba-131	11.50d	496.3	46.8	C+	T, C	Tc-96	4.28d	849.9	97.6	I	C	Rb-81	4.576h	190.3	64.0	C+	T
Ba-129m	2.17h	182.3 <sup>*1</sup>	47 <sup>*1</sup>	C+	T, C	Nb-96	23.35h	1091.3 <sup>*2</sup>	48.5 <sup>*2</sup>	I	T, C	Br-77	2.377d	520.7	22.4	C+	C
Ba-129	2.23h	214.3 <sup>*1</sup>	9.9 <sup>*1</sup>	C+	T	Nb-95	34.98d	765.8	99.8	I	T, C	As-76	1.097d	559.1	45	I	T
Ba-128	2.43d	273.4	14.5	C+	T, C	Zr-95	64.02d	756.7	54.5	C-	T, C	Se-75	119.8d	264.7	58.5	C+	T, C
Ba-126	1.67h	233.6	20	C+	T	Nb-92m	10.15d	934.5	99.1	I	C	As-74	17.77d	595.8	59.4	I	T, C
Ag-113	5.37h	298.6	10	C-	T	Sr-92	2.71h	1383.9	90	C-	T, C	Ga-73	4.86h	297.3	79.8	C-	T
Ag-112	3.130h	617.4	43	I	T	Sr-91	9.63h	749.8	23.6	C-	T, C	As-72	1.08d	834.0	79.5	I	T
Ag-110m	249.8d	657.8	94.0	I	T, C	Y-90m	3.19h	202.5	97.3	I	T, C	Ga-72	14.10h	834.0	95.6	I	T, C
Ag-106m	8.28d	717.3	28.9	I	T	Zr-89	3.267d	909.1	99.9	C+	T, C	Zn-72	1.94d	144.7	82.9	C-	T, C
Ag-105	41.29d	344.5	41.4	C+	T	Zr-88	83.4d	392.9 <sup>*2</sup>	97.3 <sup>*2</sup>	C+	T, C	As-71	2.720d	175.0	82	C+	T
Rh-105	1.473d	318.9	19.2	C-	C	Y-88	106.7d	898.0	93.7	I	T, C	Zn-71m	3.96h	386.3	93	C-	T, C
Ru-105	4.44h	724.3	47.3	C-	C	Y-87m	13.37h	380.8	78.1	C+	T	Zn-69m	13.76h	438.6	94.8	I	T
Ag-104	1.15h	767.6	66	I	T	Y-87	3.33d	484.8	89.7	C+	T, C	Ni-66	2.28d	D1039.2	7.4	C-	T
Ag-103	1.10h	118.7	31	C+	T	Sr-87m	2.803h	388.5	82.1	I	T	Ni-65	2.517h	1481.8	23.6	C-	T, C
Ru-103	39.26d	497.1	90.9	C-	T, C	Rb-86	18.63d	1077.0	8.64	I	T, C	Fe-59	44.50d	1099.3	56.5	C-	T, C
Mo-99	2.748d	D140.5	90.7	C-	T, C	Rb-84	32.77d	881.6	69.0	I	T, C	Mn-56	2.579h	846.8	98.9	C-	C
Nb-98b	51.3min	787.4	93.4	I	T	Sr-83	1.350d	762.7	30	C+	T	Sc-46	83.79d	889.3	100	I	C
Ru-97	2.9d	215.7	85.6	C+	C	Rb-83	86.2d	520.4	44.7	C+	T, C	K-43	22.3h	617.5	79.2	C-	T
Nb-97	1.20h	657.9	98.4	I	T	Rb-82m	6.472h	776.5	84.4	I	T	K-42	12.36h	1524.7	18.1	I	T
Zr-97	16.91h	743.4	93.1	C-	T, C	Br-82	1.471d	698.4	28.5	I	C	Na-24	14.96h	2754.0	100	C-	C

Nuclear data are from Ref. 23 except for \*1 from Ref. 25 and \*2 from Ref. 24.

\*3: I: independent; C-: cumulative by  $\beta^-$  decay; C+: cumulative by  $\beta^+$  decay and/or electron capture.

\*4: Identifications in Au target (T) or Mylar catcher (C).

D:  $\gamma$ -ray of the daughter in equilibrium.

### 3. Results and Discussion

**3.1. Recoil Fractions and Effective Mean Ranges.** In the present work the radioactivities of 37 product nuclides in the mass range of  $A = 24$ –131 were identified both in the forward and backward catcher foils. They are denoted with a label “C” in Table 1. In the nondestructive Au target and/or the chemically separated samples, the radioactivities of 50 nuclides in the mass range of  $A = 42$ –131 were identified as denoted with a label “T” in the same table. From the fractions of each nuclide which has recoiled out of a Au target of thickness  $W$  in unit of  $\mu\text{g}/\text{cm}^2$  into the forward and backward catcher foils, expressed as  $F = N_F/(N_F + N_B + N_{\text{target}})$  and  $B = N_B/(N_F + N_B + N_{\text{target}})$ ,  $N$  being the number of atoms, respectively, the effective mean ranges,  $FW$  and  $BW$ , in Au were obtained. Because the chemical separations of scandium and sodium were not performed in the present work, the radioactivities of  $^{46}\text{Sc}$  and  $^{24}\text{Na}$  were detected only in the catcher foils. Therefore, their mean ranges were calculated by estimating the produced activities in the target on the basis of our yield data at the same  $E_0$ .<sup>6</sup>

In Figure 1, the  $FW$  and  $BW$  values for some representative products widely separated in mass,  $^{103}\text{Ru}$ ,  $^{90\text{m}}\text{Y}$ ,  $^{74}\text{As}$ , and  $^{59}\text{Fe}$ , are shown as a function of  $E_0$  by open and closed circles, respectively. The  $FW$  and  $BW$  values seem to be independent of  $E_0$  at the studied energies, as indicated by solid and dashed lines, respectively, in Figure 1. This  $E_0$ -independence of  $FW$  and  $BW$  is coincident with those found for the typical photospallation products.<sup>1–3,12–14</sup> It is also noted that their reaction yields increase steeply with an increase of  $E_0$  up to 600 MeV and gradually at higher energies, and that the charge and mass yield parameters in the photofission of  $^{197}\text{Au}$  (Refs. 3, 7) are independent of  $E_0$  above 600 MeV. These observations indicate that the photons responsible for the production of these nuclides are mostly of energies lower than 600 MeV, (3,3)

resonance, and that there is no appreciable change in the reaction mechanism above 600 MeV; the limiting behavior. Therefore, the following discussion proceeds on the basis of the average quantities at  $E_0 \geq 600$  MeV. The average values of  $FW$  and  $BW$  are given in unit of  $\mu\text{g}/\text{cm}^2$  of Au in the 4th and 5th columns of Table 2. The quoted uncertainties represent the standard deviations in the weighted means, as determined from replicate experiments at different  $E_0$  above 600 MeV. The average forward-to-backward ratios ( $F/B$ ) at  $E_0 \geq 600$  MeV are also given in the 6th column in the same table. The results for  $^{131}\text{Ba}$ ,  $^{129\text{m}}\text{Ba}$ ,  $^{128}\text{Ba}$ , and  $^{46}\text{Sc}$  were obtained from the separate irradiation at  $E_0 = 1000$  MeV as mentioned above.

The mean ranges  $FW$  and  $BW$  at  $E_0 \geq 600$  MeV are indicated by open and closed circles, respectively, as a function of the mass difference  $\Delta A$  between a product ( $A$ ) and the target ( $A_t = 197$ ) in Figure 2. The previous results of the 20 photospallation products in the range of  $\Delta A \leq 45$  (Ref. 14) are also included in Figure 2 by the same symbols. The  $FW$  and  $BW$  are connected by solid and dashed lines, respectively. At  $\Delta A \leq 45$  the  $FW$  is about three times higher than the corresponding  $BW$ , and both increase in parallel with an increase of  $\Delta A$ . This increasing trend can be divided into two components: one is a steep exponential increase for the  $(\gamma, xn)$  ( $x \geq 1$ ) reaction products,  $^{196}\text{Au}$ ,  $^{194}\text{Au}$ , and  $^{192}\text{Au}$ ; the other is a gradual increase for the  $(\gamma, xnyp)$  ( $x, y \geq 1$ ) reaction products. The variation of the mean ranges at  $\Delta A > 45$ , however, is quite different from that found at  $\Delta A \leq 45$ . The  $FW$  and  $BW$  values are almost equal and both increase slightly with an increase of  $\Delta A$ , though those of  $^{24}\text{Na}$  ( $\Delta A = 173$ ) are somewhat higher than the values extrapolated from the increasing trend at lower  $\Delta A$ .

The forward-to-backward ratios ( $F/B$ ) at  $E_0 \geq 600$  MeV are plotted by open circles as a function of  $\Delta A$  in Figure 3. The  $F/B$  ratio represents the extent of forward peaking of the recoil, and thus is a simplified measure of the angular distribution of

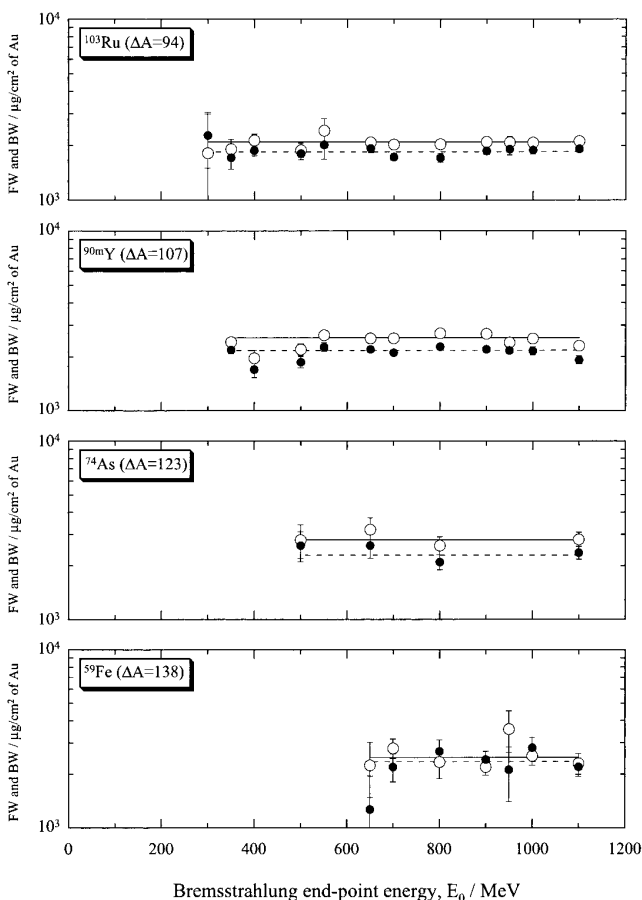


**Figure 1.** Observed mean ranges,  $FW$  (open circles) and  $BW$  (closed circles), for  $^{103}\text{Ru}$ ,  $^{90\text{m}}\text{Y}$ ,  $^{74}\text{As}$ , and  $^{59}\text{Fe}$  as a function of bremsstrahlung end-point energy,  $E_0$ .

**TABLE 2: Averaged Recoil Properties of Photofission Products from  $^{197}\text{Au}$  at  $E_0 \geq 600$  MeV**

Nuclide	$\Delta A$	TYPE*	$FW$ ( $\mu\text{g}/\text{cm}^2$ )	$BW$ ( $\mu\text{g}/\text{cm}^2$ )	$F/B$	T (MeV)
Ba-131	66	C+	$1400 \pm 400$	$550 \pm 310$	$2.6 \pm 1.6$	$17 \pm 4$
Ba-129m	68	C+	$1400 \pm 700$	$880 \pm 450$	$1.6 \pm 1.0$	$23 \pm 7$
Ba-128	69	C+	$1200 \pm 600$	$960 \pm 510$	$1.2 \pm 0.9$	$22 \pm 6$
Ag-110m	87	I	$2300 \pm 1190$	$1550 \pm 1070$	$1.48 \pm 1.28$	$54.7 \pm 16.6$
Rh-105	92	C-			$1.10 \pm 0.10$	
Ru-105	92	C-			$1.04 \pm 0.23$	
Ru-103	94	C-	$2080 \pm 500$	$1840 \pm 100$	$1.13 \pm 0.07$	$54.4 \pm 1.1$
Mo-99	98	C-	$2300 \pm 600$	$2000 \pm 500$	$1.2 \pm 0.5$	$63 \pm 9$
Ru-97	100	C+			$1.3 \pm 0.3$	
Zr-97	100	C-	$1900 \pm 500$	$1900 \pm 300$	$1.0 \pm 0.4$	$47 \pm 6$
Te-96	101	I			$0.856 \pm 0.213$	
Nb-96	101	I	$2100 \pm 200$	$1900 \pm 200$	$1.1 \pm 0.2$	$53 \pm 3$
Nb-95	102	I	$2900 \pm 400$	$2600 \pm 300$	$1.1 \pm 0.2$	$97 \pm 7$
Zr-95	102	C-	$2000 \pm 500$	$1900 \pm 300$	$1.1 \pm 0.4$	$50 \pm 6$
Nb-92m	105	I			$0.994 \pm 0.235$	
Sr-92	105	C-	$2460 \pm 680$	$2320 \pm 150$	$1.06 \pm 0.31$	$69.9 \pm 7.2$
Sr-91	106	C-	$2440 \pm 260$	$2600 \pm 540$	$0.939 \pm 0.220$	$77.7 \pm 6.6$
Y-90m	107	I	$2550 \pm 150$	$2160 \pm 120$	$1.18 \pm 0.10$	$71.9 \pm 2.1$
Zr-89	108	C+	$2300 \pm 300$	$2000 \pm 200$	$1.2 \pm 0.2$	$64 \pm 4$
Zr-88	109	C+	$2000 \pm 1000$	$1900 \pm 900$	$1.1 \pm 0.8$	$54 \pm 14$
Y-88	109	I	$2310 \pm 340$	$1930 \pm 500$	$1.20 \pm 0.36$	$60.5 \pm 6.2$
Y-87	110	C+	$2350 \pm 130$	$1990 \pm 250$	$1.18 \pm 0.17$	$63.8 \pm 3.0$
Rb-86	111	I	$2550 \pm 410$	$2550 \pm 360$	$0.992 \pm 0.205$	$80.7 \pm 6.1$
Rb-84	113	I	$2330 \pm 420$	$2000 \pm 330$	$1.17 \pm 0.29$	$61.2 \pm 5.4$
Rb-83	114	C+	$2150 \pm 260$	$1870 \pm 160$	$1.15 \pm 0.17$	$54.0 \pm 3.0$
Br-82	115	I			$1.10 \pm 0.15$	
Br-77	120	C+			$1.12 \pm 0.49$	
Se-75	122	C+	$2200 \pm 320$	$1650 \pm 1250$	$1.33 \pm 1.03$	$49.3 \pm 11.9$
As-74	123	I	$2800 \pm 400$	$2300 \pm 300$	$1.2 \pm 0.3$	$79 \pm 6$
Ga-72	125	I	$2420 \pm 150$	$2280 \pm 150$	$1.06 \pm 0.10$	$66.9 \pm 2.2$
Zn-72	125	C-	$3100 \pm 1000$	$2800 \pm 1000$	$1.1 \pm 0.6$	$95 \pm 17$
Zn-71m	126	C-	$1900 \pm 400$	$2200 \pm 600$	$0.86 \pm 0.30$	$51 \pm 7$
Ni-65	132	C-	$2200 \pm 1800$	$2700 \pm 500$	$0.81 \pm 0.68$	$69 \pm 19$
Fe-59	138	C-	$2420 \pm 530$	$2350 \pm 520$	$1.03 \pm 0.33$	$66.0 \pm 73.3$
Mn-56	141	C-			$1.09 \pm 0.04$	
Sc-46	151	C-	$3130 \pm 1390$	$3800 \pm 1660$	$0.823 \pm 0.478$	$98.1 \pm 21.9$
Na-24	173	C-	$5800 \pm 1300$	$5800 \pm 800$	$1.0 \pm 0.3$	$78 \pm 4$

\*I: independent; C-: cumulative by  $\beta^-$  decay; C+: cumulative by  $\beta^+$  decay and/or electron capture.

the product nuclei. As found previously,<sup>12-14</sup> the  $F/B$  ratio for typical photospallation products at  $E_0 \geq 600$  MeV is independent of  $\Delta A$  and also of  $A_r$ . The weighted mean value of  $F/B$  for  $^{197}\text{Au}$  at  $\Delta A \leq 45$  is  $2.5 \pm 0.6$  as indicated by a dashed line in Figure 3. The  $F/B$  values at  $\Delta A \geq 66$  obtained in the present work are also independent of  $\Delta A$  within the experimental errors. The weighted mean value of  $F/B = 1.1 \pm 0.1$  as shown by a solid line in Figure 3 is apparently lower than that for the photospallation products at  $\Delta A \leq 45$ , indicating the isotropic angular distribution of the product nuclei, which is characteristic of the two-body breakup processes such as fission or fragmentation. It is noted that this constant  $F/B$  ratio at  $\Delta A \geq 66$  reasonably agrees with the literature data of  $F/B = 1.18$  determined by Kroon and Forkmann<sup>26</sup> in the glass detector measurements of the photofission of  $^{197}\text{Au}$  at  $E_0 = 600\text{--}800$  MeV.

The proton results by Cumming and Bächmann<sup>27</sup> at proton energy  $E_p = 28$  GeV, Ross and Bächmann<sup>28</sup> at  $E_p = 0.58$  GeV, Kaufmann et al.<sup>29</sup> at  $E_p = 1, 3, 11.5, 28,$  and  $300$  GeV, and Cole and Porile<sup>30</sup> at  $E_p = 400$  GeV are included in Figure 3 by the different symbols as shown in the inset of the figure. The  $F/B$  ratios at  $E_p = 0.58, 1,$  and  $3$  GeV, which are shown by open symbols, are apparently higher than those at the higher  $E_p$  shown by closed symbols and also those of the photon-reaction at  $E_0 \geq 600$  MeV (open circles). The  $F/B$  ratios at  $E_p \leq 3$  GeV increase with an increase of  $\Delta A$  and reach peaks around  $\Delta A = 40$  at  $E_p = 1$  GeV and around  $\Delta A = 55$  at  $E_p = 3$  GeV. After the peak, the  $F/B$  decreases with an increase of  $\Delta A$  and almost levels off at  $\Delta A \geq 87$ , though a small minimum of  $F/B$  appears around  $\Delta A = 130$ . The  $F/B$  values of the proton-reactions decrease with an increase of  $E_p$  up to  $E_p = 3$  GeV, but becomes

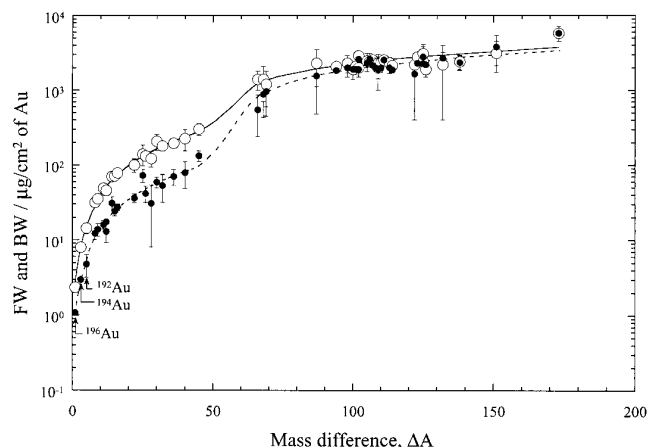


**Figure 2.** Averaged mean ranges,  $FW$  (open circles) and  $BW$  (closed circles), at  $E_0 = 600\text{--}1100$  MeV as a function of the mass difference ( $\Delta A$ ) between a product ( $A$ ) and Au target ( $A_r = 197$ ). Solid and dashed lines are drawn through the  $FW$  and  $BW$  points, respectively, to guide the eye.

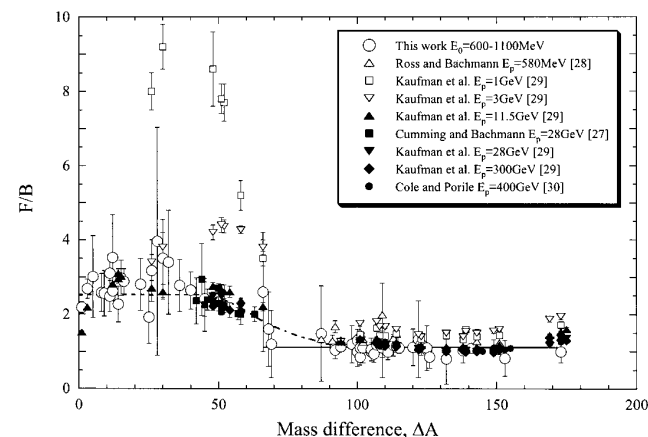


**Figure 3.** Forward-to-backward ratios ( $F/B$ ) at  $E_0 = 600\text{--}1100$  MeV as a function of the mass difference  $\Delta A$ . See text for the details.

$E_p$ -independent at the higher  $E_p$  (closed symbols). It seems interesting to note that the  $E_p$ -independent  $F/B$  values of the proton-reactions at  $E_p \geq 11.5$  GeV are equal to those of the photon-reaction at  $E_0 = 600\text{--}1100$  MeV except for the results of  $^{196}\text{Au}$  and  $^{194}\text{Au}$  produced by the simple  $(\gamma, n)$  and  $(\gamma, 3n)$  reactions, respectively.

**3.2. Kinetic Energy,  $T$ .** The measured quantities of  $FW$  and  $BW$  were used to derive the kinetic energies  $T$  of the product nuclei by means of the vector velocity model embodying the two-step mechanism commonly invoked in high-energy proton reactions. Here the two-step vector analysis developed by Winsberg<sup>15</sup> was employed for this purpose. This analytical method was successfully applied in the previous recoil studies on the photospallations on  $^{27}\text{Al}$ ,  $^{nat}\text{V}$ ,  $^{nat}\text{Cu}$ ,  $^{93}\text{Nb}$ ,  $^{nat}\text{Ag}$ ,  $^{nat}\text{Ta}$ , and  $^{197}\text{Au}$ , and the analytical details were the same as described in our previous papers.<sup>12-14</sup> The  $T$  values were calculated from the  $FW$  and  $BW$  values, and the averaged values over  $E_0 \geq 600$  MeV are given in unit of MeV in the last column of Table 2. Another recoil parameter  $v$ , which represents the forward recoil velocity from the first step, was also obtained in the present analysis, but it is out of the present discussion because they are accompanied with large errors.

The  $T$  values at  $E_0 \geq 600$  MeV are shown as a function of  $\Delta A$  by open circles, together with those of the photospallation<sup>14</sup> in Figure 4. At  $\Delta A \leq 45$  the  $T$  increases rapidly with an increase of  $\Delta A$  and shows the two components as suggested by  $FW$  and  $BW$  in Figure 2; the  $(\gamma, xn)$  ( $x \geq 1$ ) reaction products mainly produced by giant dipole resonance and the  $(\gamma, xnyp)$  ( $x, y \geq 1$ ) reaction products mainly produced by quasi-deuteron mechanism and (3,3) resonance. The increasing trend for the latter component is well explained in terms of a random-walk theory for typical spallation,<sup>27, 31</sup> in which the velocity of the product is due to the vectorial addition of the randomly directed recoil velocities resulting from multi-particle emission. In this theory, the kinetic energy  $T$  of the typical photospallation products is well systematized by a parameter  $\varepsilon_s = T/(\Delta A/A_r)$ , which represents the average kinetic energy carried off by an evaporated nucleon.<sup>31</sup> The  $\varepsilon_s$  values at  $\Delta A \leq 45$  were found to be independent of  $\Delta A/A_r$ , and the weighted mean value of  $16 \pm 5$  MeV was obtained.<sup>14</sup> The  $T$  values calculated by the PICA code<sup>16, 17</sup> at  $E_0 = 400$  MeV are also indicated by crosses for the nuclides with  $\Delta A \leq 42$ . The PICA code, which is based on the two-step model in the high-energy nuclear reaction,<sup>32</sup> can reproduce the increasing trend for the  $(\gamma, xnyp)$  products well, though the absolute values are underestimated by a factor of about 1.7 on the average for the  $(\gamma, xnyp)$  products. On the other hand, the  $T$  values at  $\Delta A \geq 87$  are quite higher than those extrapolated from the spallation trend at  $\Delta A \leq 45$  and increase slightly with an increase of  $\Delta A$  and level off around  $\Delta A = 110$ . The three  $\varepsilon_s$  values of  $^{131}\text{Ba}$  ( $\Delta A =$

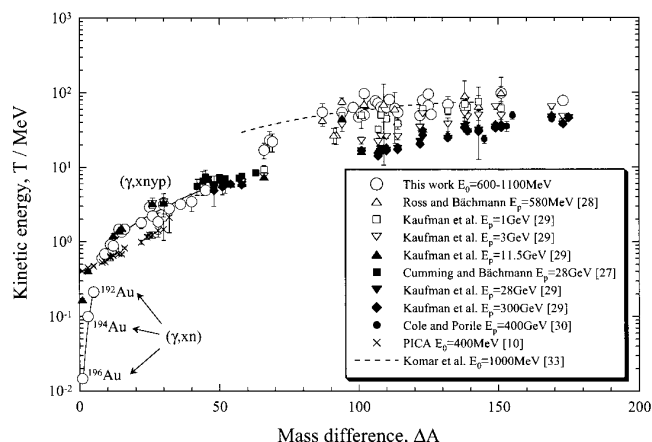


**Figure 4.** Kinetic energy,  $T$ , as a function of the mass difference  $\Delta A$ . See text for the details.

66),  $^{129\text{m}}\text{Ba}$  ( $\Delta A = 68$ ), and  $^{128}\text{Ba}$  ( $\Delta A = 69$ ) are in between the two trends. The high  $\varepsilon_s$  of more than 50 MeV imply the different reaction mechanism from typical spallation ( $\varepsilon_s = 16 \pm 5$  MeV). Komar et al.<sup>35</sup> measured the kinetic energies of coincident fragment pairs in the photofission of  $^{197}\text{Au}$  at  $E_0 = 1000$  MeV by using semiconductor detectors. Their results are shown by a dashed line in the range of  $58 \leq \Delta A \leq 142$  in Figure 4. The  $T$  values obtained radiochemically in the present work seem to be well consistent with the physical measurement by Komar et al.<sup>33</sup> except for those of the Ba isotopes at  $\Delta A = 66$ –69 as noted above. The  $T$  values of these Ba isotopes deduced in the present work are smaller by a factor of about 2 than those by Komar et al.<sup>33</sup> Since Komar et al.<sup>33</sup> employed the coincidence technique for the kinetic energy measurements, their results were confirmed to those for binary fission. The present radiochemical technique, however, can not separate the fission products from those produced from other reaction channels such as spallation and fragmentation. The smaller  $T$  values of barium isotopes may indicate that their productions are from both fission (a dashed line) and spallation (a solid line) mechanisms.

The proton results cited above<sup>27–30</sup> are also included in Figure 4 for a comparison. All of the proton data were reanalyzed in the same manner with the same range-energy relation as used in the present work in order to ensure a consistent comparison. At  $\Delta A \leq 66$  the  $T$  values from the proton-reactions are about the same with each other, irrespectively of  $E_p$ , and also with those of the photon-reaction at  $E_0 = 600$ –1100 MeV except for  $^{196}\text{Au}$ ,  $^{194}\text{Au}$ , and  $^{131}\text{Ba}$ . This similarity of the  $T$  values between the photon- and proton-reactions suggests that the mechanism of the second deexcitation step by evaporation is similar in the two types of nuclear reactions. The lower  $T$  values of  $^{196}\text{Au}$  and  $^{194}\text{Au}$  in the photon-reaction are explained by the contribution of giant dipole resonance as described in References 12 and 14. The higher  $T$  value of  $^{131}\text{Ba}$  in the photon-reaction may be due to the relatively larger contribution of fission process. The  $T$  values of  $^{131}\text{Ba}$  in the proton-induced reaction all fall on the spallation trend irrespectively of  $E_p$ , implying negligible contribution of fission process. The variation of  $T$  for the proton-reactions at  $\Delta A > 66$ , however, is quite different from that at  $\Delta A \leq 66$ . The  $T$  values of the proton-reaction products decrease with an increase of  $E_p$  and become almost constant at  $E_p \geq 11.5$  GeV (closed symbols). This decreasing trend for the proton-induced reaction is explained as a change in the reaction mechanism from binary fission to deep-spallation.<sup>34</sup> It is noted that the  $E_p$ -independent  $T$  values at  $E_p \geq 11.5$  GeV are well extrapolated

from the increasing trend of typical ( $\gamma$ , xnyp) products at  $\Delta A \leq 66$  (a solid curve). In the case of the photon-reaction, the effective photon energies are lower than 600 MeV and the variation of the  $T$  value is not found above  $E_0 = 600$  MeV. It is interesting to note that the  $T$  values from the proton-induced fission by Ross and Bächmann<sup>28</sup> at  $E_p = 580$  MeV are well coincident with the present photon-results above  $\Delta A \geq 87$ .

**3.3. Recoil Properties of  $^{24}\text{Na}$ .** Recoils of  $^{24}\text{Na}$  make it possible to trace how the production mechanism for light nuclei changes with target mass ( $A_t$ ). Many recoil studies of  $^{24}\text{Na}$  produced by various hadrons have been reported in the wide ranges of target mass and projectile energy.<sup>29–31, 35–37</sup> A few works on the photoproduction of  $^{24}\text{Na}$  have also been reported by Järund and Forkman<sup>38</sup> on  $^{\text{nat}}\text{Cu}$ ,  $^{\text{nat}}\text{Ag}$ , and  $^{197}\text{Au}$  at  $E_0 = 800$  MeV, and by Amroyan et al.<sup>39</sup> on  $^{27}\text{Al}$ ,  $^{\text{nat}}\text{Cu}$ ,  $^{\text{nat}}\text{Ag}$ , and  $^{\text{nat}}\text{Ta}$  at  $E_0 = 4.5$  GeV. Recently the recoil properties of  $^{24}\text{Na}$  from  $^{27}\text{Al}$ ,  $^{\text{nat}}\text{V}$ , and  $^{\text{nat}}\text{Cu}$  were reported by our group at  $E_0 = 600$ –1100 MeV.<sup>12–14</sup> Our  $F/B$  ratios of  $^{24}\text{Na}$  produced from  $^{27}\text{Al}$ ,  $^{\text{nat}}\text{V}$ ,  $^{\text{nat}}\text{Cu}$ , and  $^{197}\text{Au}$  are shown in Figure 5 by open circles as a function of  $A_t$ , and compared with those reported by Järund and Forkman<sup>38</sup> at  $E_0 = 800$  MeV (closed triangles) and by Amroyan et al.<sup>39</sup> at  $E_0 = 4.5$  GeV (closed squares). In addition the measurement on  $^{\text{nat}}\text{Ag}$  was performed by our group at  $E_0 = 950$  MeV and 1000 MeV, and the weighted mean value of  $F/B = 1.7 \pm 0.5$  is also included in the same figure. The results by the different authors at different incident photon energies seem to well agree with each other, indicating the characteristic limiting feature of photonuclear reaction above 600 MeV. The  $F/B$  values for  $^{27}\text{Al}$ ,  $^{\text{nat}}\text{V}$ , and  $^{\text{nat}}\text{Cu}$  targets are about 2 and consistent with the photospallation trend as found in a previous work.<sup>14</sup> However, the  $F/B$  values decrease gradually with an increase of  $A_t$ , as a whole and attain to almost unity for  $^{\text{nat}}\text{Ta}$  and  $^{197}\text{Au}$ . This variation implies that the change of the angular distribution of  $^{24}\text{Na}$  from the forward-peaking distribution to the isotropic distribution when the target mass number increases.

It may also be interesting to compare the observed mean kinetic energy  $T$  of  $^{24}\text{Na}$  with the energy  $E_C$  acquired by Coulomb repulsion in the two-body breakup process.<sup>35</sup> The ratio of  $T$  to  $E_C$  would be small if  $^{24}\text{Na}$  is produced as a residue of nucleon evaporation (spallation), and would be of the order of unity if the kinetic energy of  $^{24}\text{Na}$  is acquired as a results of Coulomb repulsion in the two-body breakup process (fission or fragmentation). The  $T/E_C$  ratios are shown as a function of  $A_t$  in Figure 6. The  $T/E_C$  ratios are about 0.5 for  $^{27}\text{Al}$ ,  $^{\text{nat}}\text{V}$ , and  $^{\text{nat}}\text{Cu}$ , and are almost unity for  $^{\text{nat}}\text{Ag}$  and  $^{197}\text{Au}$ . The variations of  $F/B$  and  $T/E_C$  with  $A_t$  may be explained as a result of the

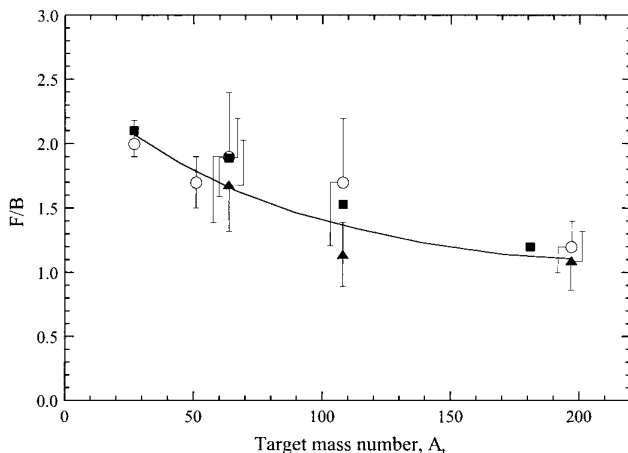


**Figure 5.** Forward-to-backward ratios ( $F/B$ ) for  $^{24}\text{Na}$  produced from  $^{27}\text{Al}$ ,  $^{\text{nat}}\text{V}$ ,  $^{\text{nat}}\text{Cu}$ ,  $^{\text{nat}}\text{Ag}$ ,  $^{\text{nat}}\text{Ta}$ , and  $^{197}\text{Au}$  at  $E_0 = 600$ –1100 MeV as a function of target mass number,  $A_t$ . The present results are shown by open circles, and those reported by Järund and Forkman<sup>38</sup> at  $E_0 = 800$  MeV and by Amroyan et al.<sup>39</sup> at  $E_0 = 4.5$  GeV are shown by closed triangles and closed squares, respectively.

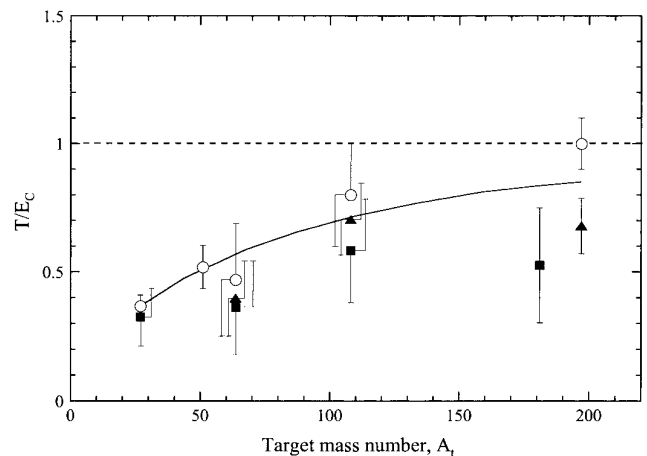


**Figure 6.** Ratios  $T/E_C$  for  $^{24}\text{Na}$  at  $E_0 = 600$ –1100 MeV as a function of target mass number  $A_t$ . The present results are shown by open circles, and those reported by Järund and Forkman<sup>38</sup> at  $E_0 = 800$  MeV and by Amroyan et al.<sup>39</sup> at  $E_0 = 4.5$  GeV are shown by closed triangles and closed squares, respectively.

transition of the reaction mechanism from spallation to fission or fragmentation. As mentioned above the kinetic energy  $T$  of typical photospallation products is well parameterized by  $\epsilon_s$ ; the  $\epsilon_s$  values are all in the range of 10–20 MeV for typical spallation products from various targets with  $A_t = 27$ –197.<sup>14</sup> The  $\epsilon_s$  values for  $^{24}\text{Na}$  from  $^{27}\text{Al}$ ,  $^{nat}\text{V}$ , and  $^{nat}\text{Cu}$  are  $11.9 \pm 1.4$ ,  $18.9 \pm 3.1$ , and  $21 \pm 10$  MeV, respectively, and they agree with the spallation trend. However, the  $\epsilon_s$  values of  $51 \pm 13$  MeV for  $^{nat}\text{Ag}$  and  $96 \pm 11$  MeV for  $^{197}\text{Au}$  are quite high compared with those for the lighter targets, implying the different reaction mechanism from spallation. It is also noted that the existence of two nuclear processes in the photoproduction of  $^{24}\text{Na}$  was found previously in the mass dependence of the reaction yields;<sup>39,40</sup> the yields decrease exponentially with an increase of  $A_t$  (spallation), but suddenly change the slope to a gradual increase around  $A_t = 100$  (fragmentation). Recently, the yields of  $^7\text{Be}$ ,  $^{22,24}\text{Na}$ , and  $^{28}\text{Mg}$  from  $^{197}\text{Au}$  was measured in our group,<sup>6</sup> and it was found that they are more than one order of magnitude higher than those extrapolated from the mass yield curve of fission, indicating a different reaction mechanism from fission; fragmentation.

As shown in Figure 4, the kinetic energy  $T$  of  $^{24}\text{Na}$  ( $\Delta A = 173$ ) produced from  $^{197}\text{Au}$  is higher by a factor of about 2 than those of the proton-induced reactions which are almost constant in the large  $\Delta A$  region, irrespectively of  $E_p$ . Also noted is that the  $F/B$  ratio of  $^{24}\text{Na}$  shown in Figure 3 is apparently smaller than those of the proton-reactions, where the  $F/B$  ratios decrease with an increase of  $E_p$ . These variations of  $T$  and  $F/B$  may imply the difference in the production mechanism of  $^{24}\text{Na}$  between the photon- and proton-reactions, though the measurements below  $E_p = 1$  GeV are required.

**Acknowledgment.** The authors would like to express their gratitude to Drs. H. Okuno and K. Masumoto, and the ES crew members of the High Energy Accelerator Research Organization at Tanashi, for their invaluable cooperations in the course of experiments. This work was supported in part by the Grant-in-Aid for Scientific Research (07304077) of the Ministry of Education, Science and Culture of Japan.

## References

- (1) S. Shibata, M. Imamura, T. Miyachi, M. Mutou, K. Sakamoto, Y. Hamajima, M. Soto, Y. Kubota, M. Yoshida, and I. Fujiwara, *Phys. Rev. C* **35**, 254 (1987).
- (2) S. R. Sarkar, M. Soto, Y. Kubota, M. Yoshida, T. Fukasawa, K. Matsumoto, K. Kawaguchi, K. Sakamoto, S. Shibata, M. Furukawa, and I. Fujiwara, *Radiochim. Acta* **55**, 113 (1991).
- (3) S. R. Sarkar, Y. Kubota, T. Fukasawa, K. Kawaguchi, K. Sakamoto, S. Shibata, and I. Fujiwara, *Radiochim. Acta* **55**, 139 (1991).
- (4) S. R. Sarkar, Y. Oura, K. Kawaguchi, A. Yazawa, K. Sakamoto, S. Shibata, and I. Fujiwara, *Radiochim. Acta* **62**, 7 (1993).
- (5) S. Shibata, M. Imamura, K. Sakamoto, S. Okizaki, S. Shibutani, H. Matsumura, M. Furukawa, I. Fujiwara, H. Nagai, and K. Kobayashi, *Radiochim. Acta* **80**, 181 (1998).
- (6) H. Matsumura, K. Washiyama, H. Haba, Y. Miyamoto, Y. Oura, K. Sakamoto, S. Shibata, M. Furukawa, I. Fujiwara, H. Nagai, T. Kobayashi, and K. Kobayashi, *Radiochim. Acta* **88**, 313 (2000).
- (7) H. Haba, M. Igarashi, K. Washiyama, H. Matsumura, M. Yamashita, K. Sakamoto, Y. Oura, S. Shibata, M. Furukawa, and I. Fujiwara, *J. Nucl. Radiochem. Sci.*, **1**, 53 (2000).
- (8) K. Sakamoto, M. Yoshida, Y. Kubota, T. Fukasawa, A. Kunugise, Y. Hamajima, S. Shibata, and I. Fujiwara, *Nucl. Phys. A* **501**, 693 (1989).
- (9) K. Sakamoto, Y. Hamajima, M. Soto, Y. Kubota, M. Yoshida, A. Kunugise, M. Masatani, S. Shibata, M. Imamura, M. Furukawa, and I. Fujiwara, *Phys. Rev. C* **42**, 1545 (1990).
- (10) Y. Oura, A. Yazawa, M. Yoshida, S. R. Sarkar, K. Sakamoto, S. Shibata, I. Fujiwara, and M. Furukawa, *Radiochim. Acta* **68**, 27 (1995).
- (11) K. Sakamoto, S. R. Sarkar, Y. Oura, H. Haba, H. Matsumura, Y. Miyamoto, S. Shibata, M. Furukawa, and I. Fujiwara, *Phys. Rev. C* **59**, 1497 (1999).
- (12) H. Haba, H. Matsumura, Y. Miyamoto, K. Sakamoto, Y. Oura, S. Shibata, M. Furukawa, and I. Fujiwara, *J. Radioanal. Nucl. Chem.* **239**, 133 (1999).
- (13) H. Haba, H. Matsumura, K. Sakamoto, Y. Oura, S. Shibata, M. Furukawa, and I. Fujiwara, *Radiochim. Acta* **85**, 1 (1999).
- (14) H. Haba, H. Matsumura, K. Sakamoto, Y. Oura, S. Shibata, M. Furukawa, and I. Fujiwara, *Radiochim. Acta* **88**, 375 (2000).
- (15) L. Winsberg, *Nucl. Instrum. Methods* **150**, 465 (1978).
- (16) T. A. Gabriel and R. G. Alsmiller Jr., *Phys. Rev.* **182**, 1035 (1969).
- (17) T. A. Gabriel, M. P. Guthrie, and O. W. Hermann, *Oak Ridge National Laboratory Report ORNL-4687* (1971).
- (18) B. Johnsson, A. Järund, and B. Forkman, *Z. Phys. A* **273**, 97 (1975).
- (19) K. Osada, T. Fukasawa, K. Kobayashi, Y. Hamajima, K. Sakamoto, S. Shibata, and I. Fujiwara, *Res. Rept. Lab. Nucl. Sci. Tohoku Univ.* **20**, 299 (1987).
- (20) H. Haba, Ph. D. Thesis (Kanazawa Univ., 1999).
- (21) Y. Hamajima (private communication, 1998).
- (22) K. Komura, *Tech. Rept. Inst. Nucl. Study, Univ. Tokyo. INS-TCH-9* (1974).
- (23) R. B. Firestone and V. S. Shirley, *Table of Isotopes*, 8<sup>th</sup> ed. (John Wiley and Sons, Inc., New York, 1996).
- (24) E. Browne and R. B. Firestone, *Table of Radioactive Isotopes*, John Wiley and Sons, Inc., New York (1986).
- (25) U. Reus and W. Westmeier, *At. Data Nucl. Data Tables* **29**, 193 (1983).
- (26) I. Kroon and B. Forkman, *Nucl. Phys. A* **179**, 141 (1972).
- (27) J. B. Cumming and K. Bächmann, *Phys. Rev. C* **6**, 1362 (1972).
- (28) E. Ross and K. Bächmann, *Radiochim. Acta* **21**, 13 (1974).
- (29) S. B. Kaufman, E. P. Steinberg, and M. W. Weisfield, *Phys. Rev. C* **18**, 1349 (1978).
- (30) G. D. Cole and N. T. Porile, *Phys. Rev. C* **25**, 244 (1982).
- (31) L. Winsberg, *Phys. Rev. C* **22**, 2116 and 2123 (1980).
- (32) R. Serber, *Phys. Rev.* **72**, 1114 (1947).
- (33) A. P. Komar, B. A. Bochagov, A. A. Kotov, Yu. N. Ranyuk, G. G. Semenchuk, G. E. Solyakin, and P. V. Sorokin, *Sov. J. Nucl. Phys.* **10**, 30 (1970).
- (34) C. F. Wang, G. D. Cole, and N. T. Porile, *Phys. Rev. C* **29**, 569 (1984).
- (35) V. P. Crespo, J. M. Alexander, and E. K. Hyde, *Phys. Rev.* **131**, 1765 (1963).
- (36) N. T. Porile and S. Tanaka, *Phys. Rev.* **135**, B122 (1964).
- (37) J. B. Cumming, P. E. Haustein, and H. -C. Hseuh, *Phys. Rev. C* **24**, 2162 (1981).
- (38) A. Järund and B. Forkman, *Z. Phys. A* **281**, 47 (1977).
- (39) K. A. Amroyan, S. A. Barsegyan, and N. A. Demekhina, *Phys. At. Nucl.* **56**, 712 (1993).
- (40) A. Järund and B. Forkman, *Z. Phys. A* **281**, 39 (1977).